A mathematical model of nutrient influence on fungal competition

M. Jabed A. Choudhury, Philip M. J. Trevelyan & Graeme P. Boswell*
Dept of Mathematics and Statistics, University of South Wales, Pontypridd, CF37 1DL, UK
*Corresponding author: graeme.boswell@southwales.ac.uk

Abstract

Fungi have a well-established role in nutrient cycling and are widely used as agents in biological control and in the remediation of polluted landscapes. Competition for resources between different fungal communities is common in these contexts and its outcome impacts on the success of such biotechnological applications. In this investigation a mathematical model is constructed to represent competition between two fungal colonies that have access to different resources. It is shown that the model equations display a multitude of travelling wave solutions and that the outcome of competition between two fungal biomasses can be controlled through the simple manipulation of the nutrient resources available to each. The model equations are also numerically integrated to illustrate the range of outcomes arising from fungal competition and these results are placed in context of established experimental observations.

Keywords: fungi; network; partial differential equation; travelling wave; phase plane.

1. Introduction

While perhaps best known for their role in nutrient cycling (Carlile et al., 2001), fungal mycelia are central to many biotechnological applications including the production of food (Efiuvweuwere and Chynyere, 2001; Flores-Maltos et al., 2011; Manjunathan et al., 2011), medicine (Luk et al., 2011; Torkelson et al., 2012; Bushley et al., 2013), the bioremediation of polluted landscapes (Sang et al., 2004; Ramachandran and Gnanados, 2013; Gupta and Shrivastava, 2014) and the biological control of crop pathogens in agriculture (Dorner et al., 2003; Cotty et al., 2007; Koutb and Ali, 2010; Mehl and Cotty, 2013; Vankudoth et al., 2016). Additionally, over 90% of plants have symbiotic connections with species of fungi enabling the acquisition of resources over far wider spatial scales than would be possible in their absence (e.g. Smith and Read, 1997; Boddy, 1999; Selosse et al., 2006). In all of these settings, fungi rarely grow in isolation and instead compete against other species for common resources including various nutrients (e.g. carbon, nitrogen and oxygen), water and even simply territory (which influences the ability of the fungus to acquire further resources). Consequently the success of any application of fungi depends on its ability to grow and suitably function in the presence of rival species.

Such interactions are usually investigated experimentally by inoculating a Petri dish with two non-mutually compatible species and observing their subsequent growth and behaviour over a range of conditions (Boddy, 2000; Evans et al., 2008). Typically the early growth of both species is radially symmetric until the periphery of the colonies collide after which one of three distinct outcomes are observed. Certain combinations of fungi display *intermingling* (also termed overgrowth or coexistence), where there is a continued and increasing overlap in the extent of both species. Other fungal pairings display *deadlock*, where neither species is able to invade territory held by the other and a stalemate is reached. The third outcome is *displacement* where one fungus takes over the territory held by the other and thereby locally eliminating its rival.

The mechanisms behind these outcomes have been well studied (e.g. Carlile et al., 2001; Utermark and Karlovsky, 2007; Sempere and Santamarina, 2010). Briefly, fungi produce a combination of volatile organic compounds (VOCs) and toxic metabolites that inhibit the growth of rivals and degrade their existing biomass (Hynes et al., 2007). Most commonly, one fungus will lyse its rival on contact as observed by the bursting of cells, the vacuolization of compartments and the withdrawal of cytoplasm (Horio and Oakley, 2005). These mechanisms are resource intensive and experimental studies have shown that the outcome of pairwise interactions is in part determined by the availability of nutrient resources (Kennedy, 2010; Mehl and Cotty, 2013). Therefore the success of any biotechnological application involving fungi depends on the provision of suitable nutrients.

However, despite the plethora of laboratory-based experimental studies, the investigation of the outcome of competition between fungal mycelia *in vivo* is complicated by the scale at which they develop. A mycelium consists of a network of microscopic tubes, termed *hyphae*, through which material, including nutrients, are transported. The extension of hyphae is the sole means by which mycelia expand and therefore the movement of *hyphal tips*, representing the apex of hyphae, are central to colony dynamics (Jackson and Heath, 1993; Gooday, 1995; Schmitz et al., 2006). The creation of hyphal tips, termed *branching*, and the fusion of hyphal tips with other hyphae, termed *amastomosis*, generates an interconnected network that is highly efficient at acquiring new resources and their resultant transportation. While hyphae typically have diameters of the order of 10 microns (Carlile et al., 2001), an entire mycelium can cover vast areas; for example, a single *Armillaria ostoyae* colony has been found to cover 900 ha (Ferguson et al., 2003). Consequently since VOCs and toxic metabolites impact at the hyphal level but their overall effects are measured at the colony level, linking these two extreme scales is difficult from a purely experimental viewpoint yet is natural in the framework of a mathematical model.

There have been a multitude of mathematical models describing fungal growth and function using continuum (e.g. Edelstein, 1982; Davidson, 1998, 2007; Davidson et al., 2011; Boswell et al., 2002, 2003; Falconer et al., 2005, 2008), discrete (e.g. Cohen, 1967; Meskauskas et al.,

2004a,b; Fuhr et al., 2011; Balmant et al., 2015), and hybrid approaches (e.g. Yang et al., 1992; Boswell et al., 2007; Schnepf et al., 2008; Davidson et al., 2011; Hopkins and Boswell, 2012; Boswell and Davidson, 2012). However the most useful models of fungal interactions have been based on continuum approaches since they efficiently represent entire fungal communities while capturing the microscopic characteristics of colony dynamics (but see Halley et al., 1994, for a cellular automaton formulation).

Davidson et al. (1996) represented a fungal mycelium and its nutrients as activators and substrates and demonstrated that spatially heterogeneous structures could be formed through the collision of two fungal biomasses; however the abstract nature of the model meant it was unable to make qualitative predictions and was difficult to differentiate between the rival biomasses. Falconer et al. (2011) formed a system of partial differential equations accounting for the interactions between rival model fungal phenotypes in response to inhibitors. Through the creation of demarcation zones, this modelling showed that such inhibitors resulted in greater fungal biodiversity. More recently, Boswell (2012) investigated pairwise competition by using an alternative continuum model whose structure and formation allowed for its calibration and it was shown that nutrient availability influenced the outcome of competition. However, due to the complexity of the underlying partial differential equations, only numerical solutions could be obtained and consequently the predictive power of the model was limited and general principles could not be extracted. In particular, repeated numerical solutions provided the only mechanism to determine critical nutrient levels to alter the outcome of competition.

The purpose of the current work is therefore to construct a mathematical model of fungal pairwise competition that simulates observed experiments and allows general principles to emerge. To maintain the generality of the model, the resource being competed for is regarded as space or territory rather than an explicit source of nutrient. Thus the outcome of competition is solely governed by independent resources available to the two fungi and this scenario is designed to reflect experiments investigating the outgrowth of fungi from isolated nutrient resources (see, for example, Tlalka et al., 2008). The model is derived in Section 2 and nondimensionalised so that 6 parameters determine its long term behaviour. In Section 3 the dynamics of the model equations are investigated through a number of analytical approaches and the results are augmented by numerical simulation. In particular, algebraic conditions are constructed that relate nutrient concentrations to the outcome of competition. The implications of the results are discussed in Section 4.

2. Modelling

In laboratory-based experiments a Petri dish is inoculated with species of fungi that expand outwards in a radially symmetric manner and the overall outcome of pairwise com-

petition is determined by observing how the colony peripheries behave immediately before and then following their collision. Thus, due to the radial symmetry involved, a one-dimensional mathematical model is sufficient to investigate such competition corresponding to the growth along the line connecting the centers of the inoculation sites.

Edelstein (1982) formulated a basic structure for the representation of fungal growth by modelling the populations of hyphae and hyphal tips and noted that the creation of hyphae corresponded to the trail left behind a moving tip. This same "tip and trail" structure has been used successfully in other investigations (e.g Boswell et al., 2002; Boswell, 2012). Thus we introduce ρ_j and n_j to denote the density of hyphae and the density of hyphal tips respectively in fungal biomass j where $j = 1, 2$ represent two different fungal phenotypes. Since the process of hyphal tip extension is the culmination of a cascade of metabolic processes each requiring suitable nutrients, consistent with previous studies (e.g. Prosser and Trinci, 1979) it is reasonably assumed that the speed of tip movement is proportional to the concentration of nutrients available to that fungal biomass. Since the purpose of the current investigation is to understand the role of nutrient availability on the outcome of competition, it is assumed that the nutrients are represented by a single generic substrate and that c_j denotes the concentration of that substrate available to biomass j. Thus the speed of the model tip movement in biomass j is denoted by $v_j c_j$ and the creation of biomass is given by the corresponding flux of the model tips. Also, to capture the natural turnover in hyphal segments, it is assumed that material in biomass j has a constant degradation rate of γ_j independent of any competition.

Hyphal tips are created by the process of branching, which can either arise through the bifurcation of an existing hyphal tip (often termed dichotomous branching) or through the emergence of a new branch midway along an established hyphal segment (termed lateral branching). In the current study attention is focussed exclusively on the more prevalent lateral branching but note that the techniques applied can be easily translated to the case of dichotomous branching. Experimental investigations have long since established that an increase in glucose concentrations within a mycelium is associated with an increase in hyphal branching (e.g. Gruhn et al., 1992). Consequently, and consistent with previous modelling studies (Boswell et al., 2003, 2007; Boswell, 2012; Hopkins and Boswell, 2012), it is assumed that the production of new model tips in biomass j is proportional to $c_j \rho_j$ capturing the dependence of this process on both the concentration of substrate and the hyphal length from which new tips can emerge. Anastomosis, the fusion of tips with other hyphae, is a process that regulates the density of hyphal tips. Again, consistent with previous studies (Edelstein, 1982; Boswell, 2012), it is assumed that the per capita loss of model tips in biomass j is proportional to the density of biomass j, namely ρ_j.

During fungal competition, combinations of VOCs and toxic metabolites are produced along the lengths of hyphae that comprise the mycelium. Due to the concomitant energy

costs, the production of these compounds is reasonably assumed to be proportional to the energy available to the biomass, i.e. proportional to c_1 or c_2. Further, since these compounds restrict the ability of a rival biomass to create new hyphal material as well as degrading existing hyphae, they essentially cause hyphal tips in a rival to cease functioning and reduce the density of existing biomass. For convenience these substances are not represented explicitly but instead their influence on rival biomasses is modelled. Therefore the process of tip inhibition/degradation and hyphal degradation in biomass j by biomass i ($i \neq j$) is modelled using terms proportional to $c_i\rho_i n_j$ and $c_i\rho_i\rho_j$ respectively. This approach is consistent with observed behaviour of competing fungi where the amount of VOCs produced changes during competition and depends on the degree of contact between the two species (Hynes et al., 2007).

Thus the mathematical model is described by four coupled partial differential equations

$$\begin{aligned}
\frac{\partial \rho_1}{\partial t} &= v_1 c_1 n_1 - \gamma_1 \rho_1 - E c_2 \rho_2 \rho_1, \\
\frac{\partial n_1}{\partial t} &= -\frac{\partial (v_1 c_1 n_1)}{\partial x} + \alpha_1 c_1 \rho_1 - \beta_1 \rho_1 n_1 - A c_2 \rho_2 n_1, \\
\frac{\partial \rho_2}{\partial t} &= v_2 c_2 n_2 - \gamma_2 \rho_2 - F c_1 \rho_1 \rho_2, \\
\frac{\partial n_2}{\partial t} &= \frac{\partial (v_2 c_2 n_2)}{\partial x} + \alpha_2 c_2 \rho_2 - \beta_2 \rho_2 n_2 - B c_1 \rho_1 n_2,
\end{aligned} \tag{1}$$

where γ_j denotes the natural loss of hyphae, α_j represents the branching rate per unit substrate, β_j represents the anastomosis rate per unit length of hyphae and A, B, E and F are the proportionality constants of the rate of degradation of biomass and associated tips due to competition and which may be different between the two biomass "phenotypes". Notice that the sign of the fluxes for the hyphal tips are reversed ensuring that both biomasses expand in opposite directions and thus will collide with suitable initial data; an approach that has successfully been used in previous studies (e.g. Boswell, 2012).

The model equations are to be solved on the spatial interval $(-L, L)$ and to be consistent with the typical experimental protocol described above require zero-flux boundary conditions because in the associated experimental configuration no material enters or leaves the Petri dish after inoculation. Furthermore, suitable initial data, representing the inoculation of the Petri dish, requires that the two rival biomasses start on opposite sides of the interval with no overlap. Hence the initial data is taken to be of the form

$$\rho_1(x,0) = \begin{cases} 0 & \text{if } x \geq 0 \\ \tilde{\rho}_1(x) & \text{otherwise} \end{cases}, \qquad \rho_2(x,0) = \begin{cases} \tilde{\rho}_2(x) & \text{if } x \geq 0 \\ 0 & \text{otherwise} \end{cases},$$
$$n_1(x,0) = \begin{cases} 0 & \text{if } x \geq 0 \\ \tilde{n}_1(x) & \text{otherwise} \end{cases}, \qquad n_2(x,0) = \begin{cases} \tilde{n}_2(x) & \text{if } x \geq 0 \\ 0 & \text{otherwise} \end{cases}, \tag{2}$$

where $\tilde{\rho}_j$ and $\tilde{n}_j$ are specified functions. Henceforth we assume biomass 1 starts on the left hand side of the domain and biomass 2 starts on the right hand side of the domain.

The main purpose of the current investigation is to focus on the role of nutrient availability and its involvement in determining the outcome of pairwise competition between fungi. As previous studies have shown (e.g. Edelstein, 1982), tip velocity and local branching and anastomosis rates dictate the densities achieved by biomasses in the absence of competition which in turn impact on the competitive ability of the biomass. Therefore, in order to isolate the key role of nutrient availability on competition, it is reasonably assumed that the two rival biomasses have similar growth characteristics and only differ in their local nutrient resources and their ability to degrade and inhibit the growth of their rivals. Thus we henceforth set $v_1 = v_2 = v$, $\alpha_1 = \alpha_2 = \alpha$, $\beta_1 = \beta_2 = \beta$ and $\gamma_1 = \gamma_2 = \gamma$. The resultant model equations (1) can be nondimensionalised by introducing $\rho_j^* = \frac{\rho_j \beta\gamma}{\alpha v}$, $n_j^* = \frac{n_j \beta}{\alpha}$, $\psi = \frac{\alpha v}{\gamma^2}$, $A^* = \frac{A}{\beta}$, $B^* = \frac{B}{\beta}$, $E^* = \frac{\alpha v}{\beta\gamma^2}E$, $F^* = \frac{\alpha v}{\beta\gamma^2}F$, $x^* = \frac{\gamma x}{v}$ and $t^* = \gamma t$ giving rise to

$$\begin{aligned}
\frac{\partial \rho_1}{\partial t} &= c_1 n_1 - \rho_1 - E c_2 \rho_1 \rho_2, \\
\frac{\partial n_1}{\partial t} &= -\frac{\partial}{\partial x}(c_1 n_1) + \psi c_1 \rho_1 - \psi \rho_1 n_1 - A\psi c_2 n_1 \rho_2, \\
\frac{\partial \rho_2}{\partial t} &= c_2 n_2 - \rho_2 - F c_1 \rho_1 \rho_2, \\
\frac{\partial n_2}{\partial t} &= \frac{\partial}{\partial x}(c_2 n_2) + \psi c_2 \rho_2 - \psi \rho_2 n_2 - B\psi c_1 \rho_1 n_2,
\end{aligned} \tag{3}$$

where stars have been dropped for notational convenience. While alternative non-dimensionalisations are possible, the particular choice adopted here, which retains independent parameters relating to the two substrate concentrations, is central to the results obtained below.

Previous modelling investigations (e.g. Boswell et al., 2002, 2003) explicitly simulated the distribution of a substrate, representing a growth promoting carbon, inside the biomass structure, accounting for not only its uptake from the external environment and depletion due to growth costs, but also its movement within the biomass network. Indeed, when the external resource was continually replenished, the internally-held substrate distribution was the same order of magnitude throughout the majority of the biomass (Boswell, 2012).

Consequently, it is assumed that the variables c_1 and c_2 are constant throughout the biomass and also do not change over time corresponding to biomass expansion and competition in a continually-replenished or nutrient-rich environment.

When considered in isolation, each of the biomasses and corresponding tips from equation (3) generate a stable travelling wave solution (see below). Thus to ensure the biomasses have attained stable distributions prior to their contact, the initial distributions $\tilde{\rho}_j$ and $\tilde{n}_j$ are chosen to be similar to their travelling wave profile. Consequently, and solely for the purpose of numerical integration, the nondimensionalised version of the initial data in equation (2) is

$$\begin{aligned} \tilde{\rho}_1(x) &= \frac{c_1^2}{2}\mathrm{erfc}\left(\frac{\tilde{x}+x}{2}\right), & \tilde{n}_1(x) &= \frac{c_1}{2}\mathrm{erfc}\left(\frac{\tilde{x}+x}{2}\right), \\ \tilde{\rho}_2(x) &= \frac{c_2^2}{2}\mathrm{erfc}\left(\frac{\tilde{x}-x}{2}\right), & \tilde{n}_2(x) &= \frac{c_2}{2}\mathrm{erfc}\left(\frac{\tilde{x}-x}{2}\right), \end{aligned} \tag{4}$$

where $2\tilde{x}$ represents the initial distance between the two model biomasses and erfc is the complementary error function. Note that while these functions are not the final travelling wave profiles obtained by the biomasses when considered in isolation of each other, provided $\tilde{x}$ is sufficiently large these initial profiles quickly converge to their stable distributions before any interactions.

3. Analysis and Results

As previously explained, the suppression of hyphal tip extension and the degradation of hyphae represent the two major processes used by fungal biomasses during competition. To isolate the effect of each, attention is focussed first on the impact of tip suppression when hyphal degradation is neglected (by assuming E and F are both zero) before extending the analysis to include both processes acting simultaneously.

3.1. Biomass competition with tip suppression only

Edelstein (1982) showed that model equations similar to those in (3) gave rise to travelling wave solutions and hence if there are travelling wave solutions the spatially-uniform stationary points provide information on such solutions. Equation (3) with $E = F = 0$ has four such stationary points that can be found and classified (see Appendix). The equilibrium corresponding to the absence of both biomasses $(\rho_1, n_1, \rho_2, n_2) = (0, 0, 0, 0)$ is a saddle point. There are two stationary points corresponding to the presence of a single biomass: $(c_1^2, c_1, 0, 0)$, which is stable provided $Bc_1^3 > c_2^2$ and a saddle point otherwise, and $(0, 0, c_2^2, c_2)$, which is stable provided $Ac_2^3 > c_1^2$ and a saddle point otherwise. Finally there is a fourth stationary point corresponding to coexistence (or intermingling)

$$\left(\frac{Ac_2^3-c_1^2}{ABc_1c_2-1},\frac{Ac_2^3-c_1^2}{c_1(ABc_1c_2-1)},\frac{Bc_1^3-c_2^2}{ABc_1c_2-1},\frac{Bc_1^3-c_2^2}{c_2(ABc_1c_2-1)}\right)$$

which is biologically realistic (i.e. non-negative) and stable when both $Ac_2^3 < c_1^2$ and $Bc_1^3 < c_2^2$, biologically realistic and unstable (a saddle point) when both $Ac_2^3 > c_1^2$ and $Bc_1^3 > c_2^2$, and biologically unrealistic for other parameter combinations. Consequently the c_1-c_2 parameter space is divided into four regions by the curves $Ac_2^3 = c_1^2$ and $Bc_1^3 = c_2^2$ (Fig. 1 with $E = F = 0$). In essence, when either c_1 is significantly larger than c_2, or c_2 is significantly larger than c_1, one fungal biomass will displace the other. If both c_1 and c_2 are sufficiently large then multiple stable equilibria arise and so precise values of c_1 and c_2, along with initial data, determine the outcome of competition. Finally, if both c_1 and c_2 are similarly and sufficiently small then the only stable equilibrium corresponds to the coexistence (i.e. intermingling) of biomasses.

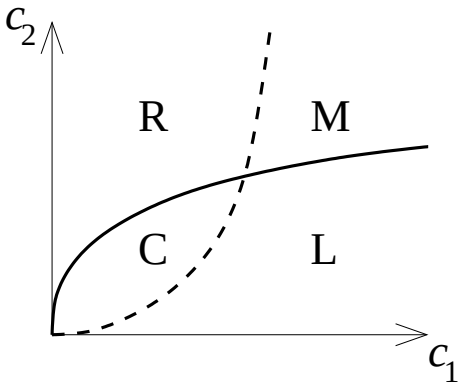

Figure 1: The c_1-c_2 parameter space for equations (3) is divided into regions by the curves $Ac_2^3(1+Ec_2^3) = c_1^2$ (solid line) and $Bc_1^3(1 + Fc_1^3) = c_2^2$ (dashed line). Region R corresponds to where the biomass initially starting on the right will displace that initially on the left. Region L corresponds to where the biomass initially starting on the left will displace that initially on the right. Region C corresponds to where coexistence (or intermingling) of biomasses arises. Region M corresponds to where multiple stable equilibria are found, which can include deadlock.

To prove the existence of travelling wave solutions, it is necessary to prove the existence of trajectories in the four-dimensional state space connecting equilibria constructed above. To this end, introduce $z = x - st$, where s is a constant corresponding to the speed of a travelling wave. Equations (3) with $E = F = 0$ can then be represented as

$$
\begin{aligned}
\rho_1' &= -\frac{1}{s}\left(c_1 n_1 - \rho_1\right), \\
n_1' &= -\frac{\psi}{s - c_1}\left(c_1\rho_1 - \rho_1 n_1 - A c_2 n_1 \rho_2\right), \\
\rho_2' &= -\frac{1}{s}\left(c_2 n_2 - \rho_2\right), \\
n_2' &= -\frac{\psi}{s + c_2}\left(c_2\rho_2 - \rho_2 n_2 - B c_1 \rho_1 n_2\right),
\end{aligned}
\tag{5}
$$

where prime denotes differentiation with respect to the wave variable z. The parameter ψ can be regarded as separating the reaction terms of equation (3) into two classes: those that change in proportion to ψ, representing the change of the hyphal tip population, and those independent of ψ, representing the change of the hyphal biomass population. For small values of ψ the change in the model variables n_1 and n_2 can be regarded as being slower than the change in both ρ_1 and ρ_2. Due to the construction of the model equations, in particular that the change in the biomass concentrations ρ_j $(j = 1, 2)$ is dictated by the movement of model tips n_j, the change in biomass concentration lags behind a change in tip concentration (effectively the biomass concentration is continually "catching up" with the tip concentration). Thus there is an inherent stability embedded in the model equations for ρ_j and therefore it is reasonable to take the approximations $\rho_1 = c_1 n_1$ and $\rho_2 = c_2 n_2$ along trajectories in the four-dimensional state space. Thus the system of equations (5) then reduce to

$$
\begin{aligned}
n_1' &= -\frac{\psi n_1}{s - c_1}\left(c_1^2 - c_1 n_1 - A c_2^2 n_2\right), \\
n_2' &= -\frac{\psi n_2}{s + c_2}\left(c_2^2 - c_2 n_2 - B c_1^2 n_1\right).
\end{aligned}
\tag{6}
$$

This pair of equations can be investigated using standard phase plane analysis. Consistent with the construction of Fig. 1, there are four distinct ways in which the nullclines of equations (6) can intersect. Additionally, the direction of flow in the phase planes of each of these instances depends on the sign of the expressions $s - c_1$ and $s + c_2$ corresponding to the three cases $s > c_1$, $-c_2 < s < c_1$ and $s < -c_2$. The twelve possible phase portraits are illustrated in Fig. 2. The existence of travelling wave solutions in model equations (3) requires the presence of trajectories in the phase portraits connecting equilibria in a meaningful manner (e.g. the direction of flow in the state space is consistent with the sign of s and corresponds to biomass expansion in the appropriate direction). In region L of the parameter space of Fig. 1 (where the biomass starting on the left displaces that on the right, and hence indicates a positive value of s), the only physically realistic trajectories

Table 1: Travelling wave solutions of equations (3) with $E = F = 0$ for small ψ.

Fig. 1 Region	Outcome	Condition	Wave speed (s)
L	Left biomass displaces right	$c_2^2 < Bc_1^3,\ Ac_2^3 < c_1^2$	$s > c_1$
M	Multiple outcomes	$c_2^2 < Bc_1^3,\ Ac_2^3 > c_1^2$	$-c_2 < s < c_1$
R	Right biomass displaces left	$c_2^2 > Bc_1^3,\ Ac_2^3 > c_1^2$	$s < -c_2$
C	Coexistence / intermingling	$c_2^2 > Bc_1^3,\ Ac_2^3 < c_1^2$	$s > c_1$ or $s < -c_2$

connecting equilibria arise when $s > c_1$ (Fig. 2(a)), thus generating a lower bound for the travelling wave speed. Notice that there are two heteroclinic trajectories in this instance representing the movement of biomass into an empty domain and the movement following collision with the biomass initially starting on the right. A similar situation arises in region R of Fig. 1, except the wave speed satisfies $s < -c_2$ (Fig. 2(k)). In region M of Fig. 1, where multiple outcomes of biomass competition are possible, the only travelling waves that can exist must satisfy $-c_2 < s < c_1$ (Fig. 2(f)). Finally, in region C of Fig. 1, corresponding to the coexistence (or intermingling) of biomasses, the only physically realistic trajectories satisfy either $s > c_1$ or $s < -c_2$ (Fig. 2(d), (l)). (Note that in Fig. 2 (e), (g) there are no heteroclinic orbits and hence no corresponding travelling waves while in Fig. 2(b, c, h, i, j) the direction of the trajectories is incompatible for the existence of travelling wave solutions for the corresponding values of s or not consistent with the stability of the four equilibria of equations (3) found above.) The resultant bounds on wave speed for the small ψ case are summarised in Table 1. Consequently, given the bounds on the wave speeds constructed above, the instance of deadlock, which corresponds to stationary distributions, can only arise for values of c_1 and c_2 lying in Region M of Fig. 1.

A similar technique can be applied when ψ is large so that it is reasonable to make the approximations $n_1 = c_1\rho_1/(\rho_1 + Ac_2\rho_2)$ and $n_2 = c_2\rho_2/(\rho_2 + Bc_1\rho_1)$ along trajectories. Under these conditions equation (5) reduces to the pair of equations

$$\begin{aligned} \rho_1' &= -\frac{\rho_1}{s(\rho_1 + Ac_2\rho_2)}\left(c_1^2 - \rho_1 - Ac_2\rho_2\right), \\ \rho_2' &= -\frac{\rho_2}{s(\rho_2 + Bc_1\rho_1)}\left(c_2^2 - \rho_2 - Bc_1\rho_1\right). \end{aligned} \tag{7}$$

As before, there are four alternative ways the nullclines can intersect and the direction of flow depends on the sign of s yeilding a total of 8 distinct phase portraits (Fig. 3). Depending on parameter values, there are trajectories connecting various equilibria similar to the previous case for small ψ but in this instance there are no restrictions on s and hence no bounds on the speed of the travelling waves can be constructed.

The model equations (3) with initial data (2), (4) were solved numerically for a range of parameter values c_1 and c_2 with $E = F = 0$ for small and large values of ψ (Figs. 4, 5, 6).

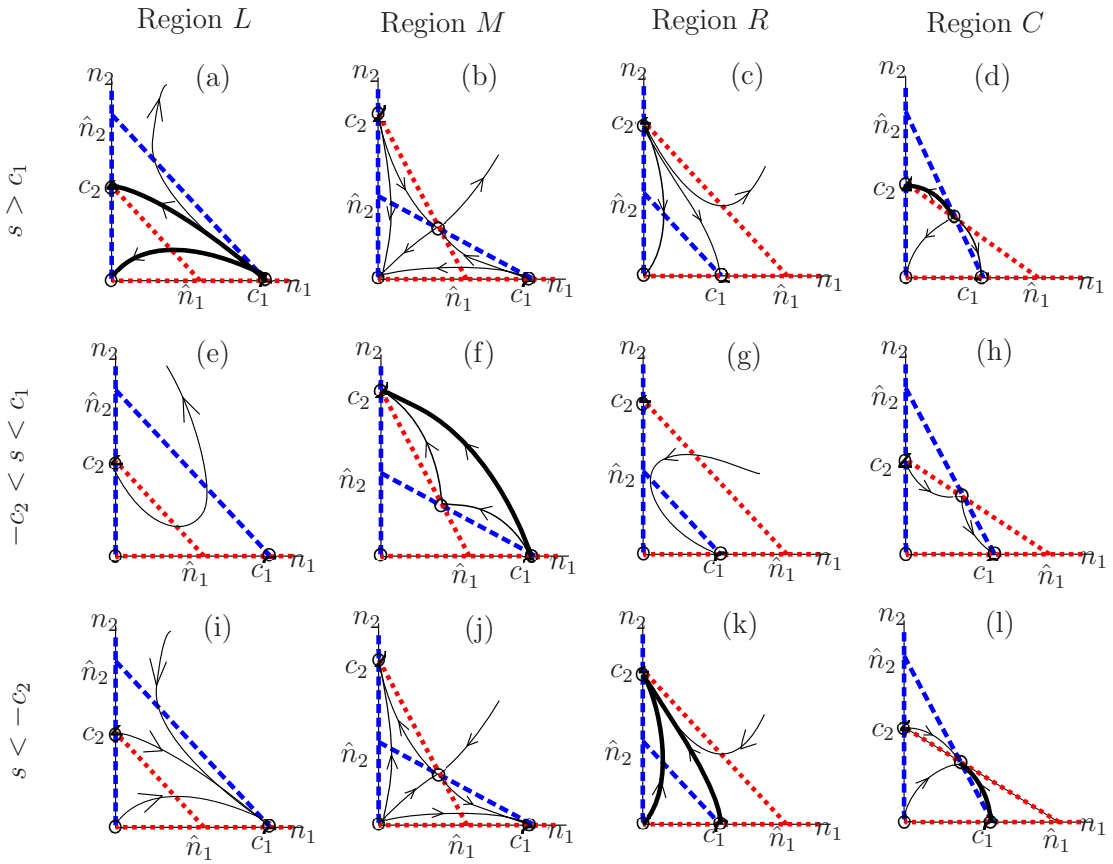

Figure 2: Phase portraits of equations (6) with small ψ for the cases outlined in Fig. 1 where s takes the values indicated and $\hat{n}_1 = c_2^2/(Bc_1^2)$, $\hat{n}_2 = c_1^2/(Ac_2^2)$. The n_1- and n_2-nullclines are represented by the dashed (blue) and dotted (red) lines respectively with typical trajectories represented by solid black lines. Trajectories in bold illustrate biologically relevant travelling wave solutions of equations (3) for small ψ with $E = F = 0$.

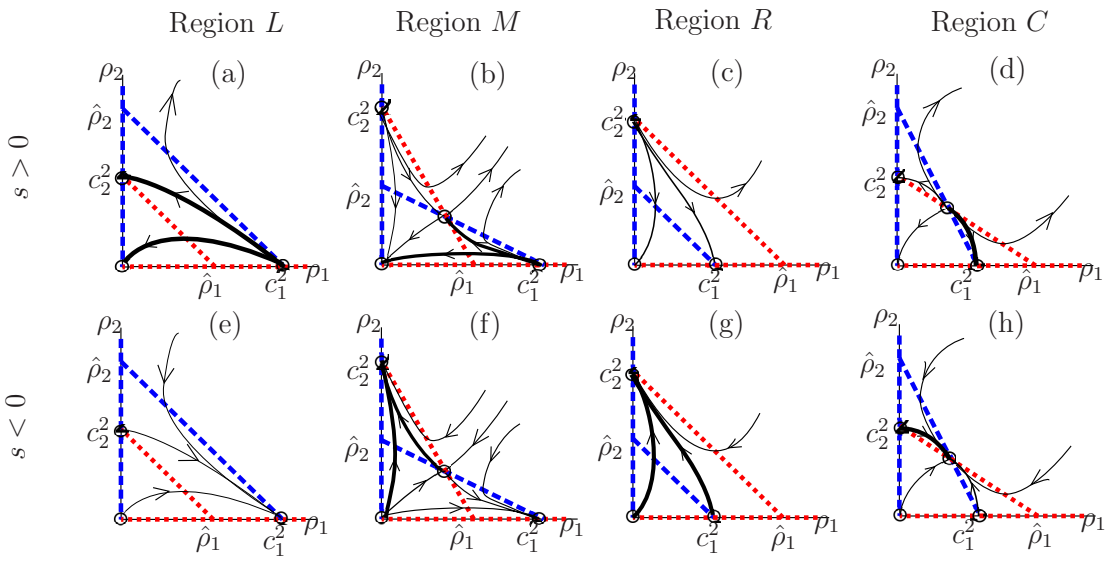

Figure 3: Phase portraits of equations (7) for the different regions of Fig. 1 where $s > 0$ and $s < 0$ as indicated and $\hat{\rho}_1 = c_2^2/(Bc_1)$, $\hat{\rho}_2 = c_1^2/(Ac_2)$. The ρ_1- and ρ_2-nullclines are represented by the dashed (blue) and dotted (red) lines respectively. Sample trajectories are indicated along with specific trajectories (in bold) connecting equilibria illustrating biologically relevant travelling wave solutions of equations (3) for large ψ with $E = F = 0$.

In all instances, the initial distributions of model biomass ρ_j and model tips n_j $(j = 1, 2)$ rapidly converged on a stable travelling wave profile taking values of zero in front of the wave and $\rho_j = c_j^2$ and $n_j = c_j$ $(j = 1, 2)$ behind it, consistent with the equilibria found above. These profiles propagated towards the centre of the domain with a constant velocity s_j $(j = 1, 2)$, that was calculated numerically, and in all cases $s_1 > c_1$ and $s_2 < -c_2$, in line with the above analysis. The leading edge of the model tips marginally preceded the leading edge of the model biomasses, which is consistent with the model structure where biomass creation was proportional to tip flux and further justifies the methodology applied in the small and large ψ analysis investigated above. The rival distributions collided with each other close to the origin but the exact position varied with the values of c_1 and c_2 due to the differences in the propagation speeds s_1 and s_2. Following their collisions, the distributions took numerous forms depending on parameter values and the speed of the travelling fronts changed accordingly.

For $\psi = 0.1$, representing a small value of this parameter, the outcome depended upon the values of A, B, c_1 and c_2. When $c_2 < A^{-3/5}B^{-2/5}$ (corresponding to the value of c_2 at the non-trivial intersection of the curves identified in Fig. 1 with $E = F = 0$) three outcomes arose consistent with the above analysis. If c_1 was sufficiently small, i.e. $c_1 < (Ac_2^3)^{1/2}$ and so in Region R of Fig. 1, then the biomass initially starting on the right displaced that initially starting on the left and a corresponding travelling wave solution arose (Fig. 4(a)) where the resultant wave speed satisfied $s < -c_2$. If $(Ac_2^3)^{1/2} < c_1 < (c_2^2/B)^{1/3}$, corresponding to Region C of Fig. 1, then the biomasses coexisted after their

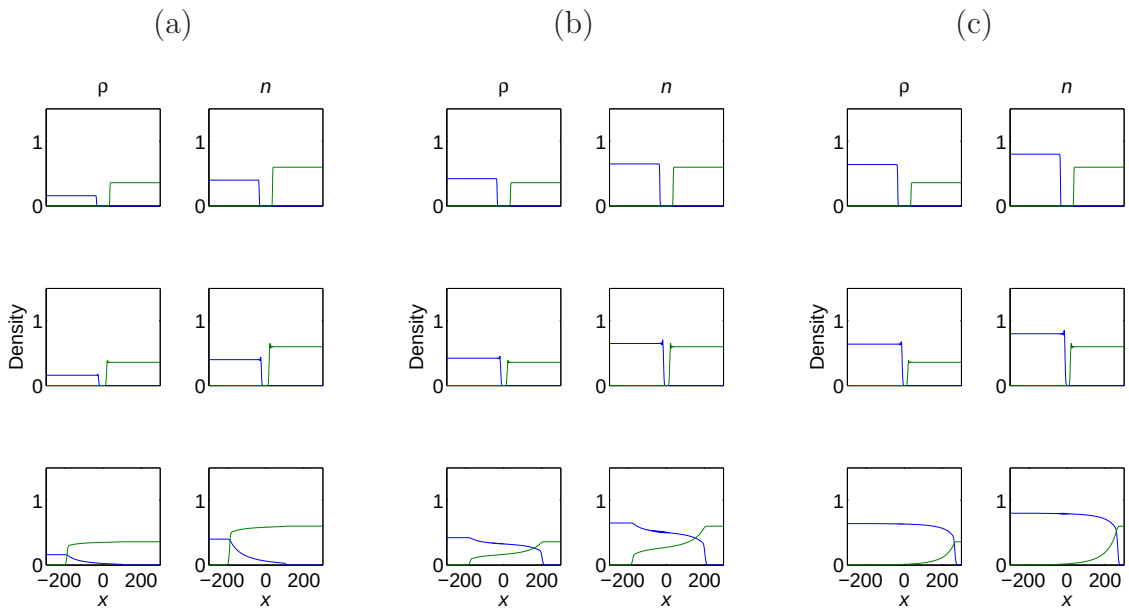

Figure 4: Numerical solutions of equations (3) with initial data (2),(4) over the interval $(-300, 300)$ with $\tilde{x} = 35$ and $A = B = 1$, $E = F = 0$ and $\psi = 0.1$. Distributions are shown at times $t = 0$, $t = 30$ and $t = 350$ where values of c_1 and c_2 belong to (a) region R, (b) region C and (c) region L of Fig. 1. (a) $c_1 = 0.4$, $c_2 = 0.6$ (with travelling wave speeds of $s_1 = 0.43, s_2 = -0.65$ before collision, $s_1 = s_2 = -0.64$ after collision). (b) $c_1 = 0.65$, $c_2 = 0.6$ (with travelling wave speeds of $s_1 = 0.72, s_2 = -0.65$ before collision, $s_1 = 0.69, s_2 = -0.61$ after collision). (c) $c_1 = 0.8$, $c_2 = 0.6$ (with travelling wave speeds of $s_1 = 0.87, s_2 = -0.65$ before collision, $s_1 = s_2 = 0.87$ after collision).

collision at reduced densities and both wave fronts continued to propagate at reduced speeds (Fig. 4(b)) where $s_1 > c_1$ and $s_2 < -c_2$. If $c_1 > (c_2^2/B)^{1/3}$, corresponding to Region L of Fig. 1, then the biomass initially starting on the left displaced that on the right (Fig. 4(c)) and the resultant wave speed satisfied $s > c_1$. When $c_2 > A^{-3/5}B^{-2/5}$, consistent with the parameter space of Fig. 1, the biomass initially starting on the right displaced that on the left if $c_1 < (c_2^2/B)^{1/3}$ (i.e. in Region R) and vice-versa if $c_1 > (Ac_2^3)^{1/2}$ (i.e. in Region L). However, for $(c_2^2/B)^{1/3} < c_1 < (Ac_2^3)^{1/2}$ (corresponding to region M in Fig. 1) different solutions were obtained depending on the precise values of c_1 and c_2 corresponding to the right biomass displacing the left (Fig. 5(a)); deadlock, where neither distribution moved following collision (Fig. 5(b)); and the left biomass displacing the right (Fig. 5(c)). In all these cases, the speeds of the travelling wave fronts satisfied $-c_2 < s < c_1$, consistent with the bounds presented in Table 1.

The bounds on the travelling wave speeds for small ψ (Table 1) do not apply to larger values of ψ (Fig. 6). For example, in Fig. 6(a), following collision of biomasses, the speed of the advancing wave fronts satisfied $s_1 > c_1$ and $s_2 < -c_2$ while in Fig. 6(c), their speeds satisfied $s_1 < c_1$ and $s_2 > -c_2$, despite both these combinations of c_1 and c_2 belonging to region C of Fig. 1.

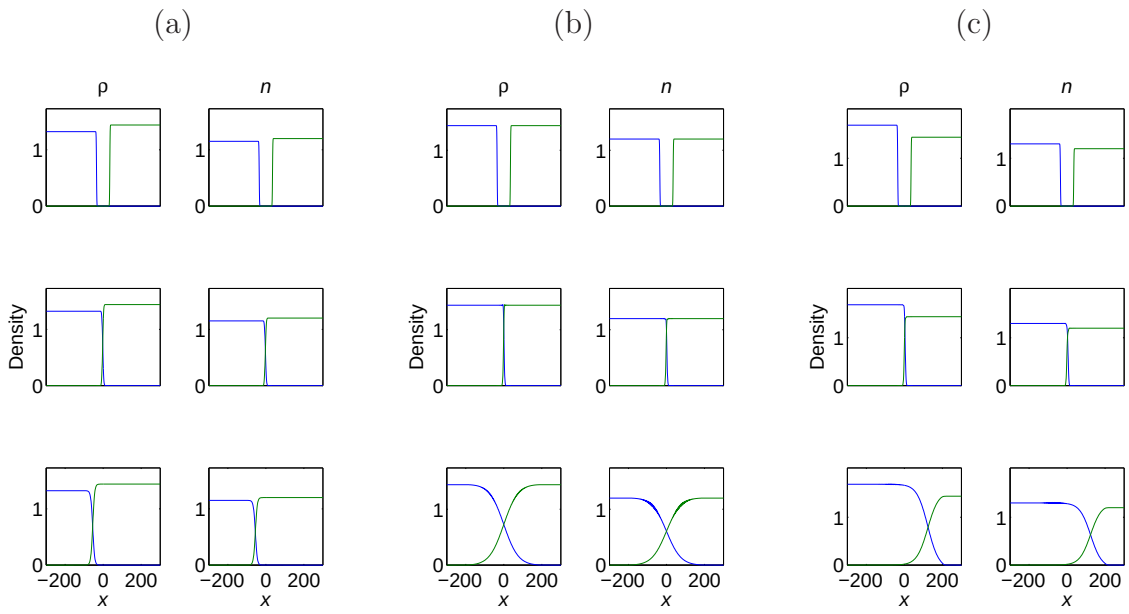

Figure 5: Numerical solutions of equations (3) with initial data (2),(4) over the interval $(-300, 300)$ with $\tilde{x} = 35$ and $A = B = 1$, $E = F = 0$ and $\psi = 0.1$. Distributions are shown at times $t = 0$, $t = 30$ and $t = 200$ where values of c_1 and c_2 belong to region M of Fig. 1, where multiple outcomes from competition are possible. (a) $c_1 = 1.15$, $c_2 = 1.2$ (with travelling wave speeds of $s_1 = 1.30, s_2 = -1.35$ before collision, $s_1 = s_2 = -0.33$ after collision). (b) $c_1 = 1.2$, $c_2 = 1.2$ (with travelling wave speeds of $s_1 = 1.35, s_2 = -1.35$ before collision, $s_1 = s_2 = 0$ after collision, i.e. deadlock). (c) $c_1 = 1.3$, $c_2 = 1.2$ (with travelling wave speeds of $s_1 = 1.59, s_2 = -1.35$ before collision, $s_1 = s_2 = 1.13$ after collision).

3.2. Biomass competition with tip suppression and hyphal degradation

When the processes of both tip suppression and hyphal degradation are considered acting simultaneously, the same qualitative features arose as obtained above. The spatially-uniform stationary points take more complicated forms and correspond to the absence of both biomasses, the presence of only one biomass, and the coexistence of biomasses. The stability of these four stationary points can be mostly determined (see Appendix). The equilibrium $(\rho_1, n_1, \rho_2, n_2) = (0, 0, 0, 0)$ is a saddle point. The stationary point $(c_1^2, c_1, 0, 0)$ is stable provided $Bc_1^3(1 + Fc_1^3) > c_2^2$ and a saddle point otherwise. The steady state $(0, 0, c_2^2, c_2)$ is stable provided $Ac_2^3(1 + Ec_2^3) > c_1^2$ and a saddle point otherwise. In general, the equilibria corresponding to coexistence cannot be expressed in closed form nor can its stability be determined except in a number of special circumstances. One insightful exception arises when $A = B = 0$ (i.e. in the absence of tip suppression) in which case the stationary point is $(\bar{\rho}_1, \bar{n}_1, \bar{\rho}_2, \bar{n}_2)$ where

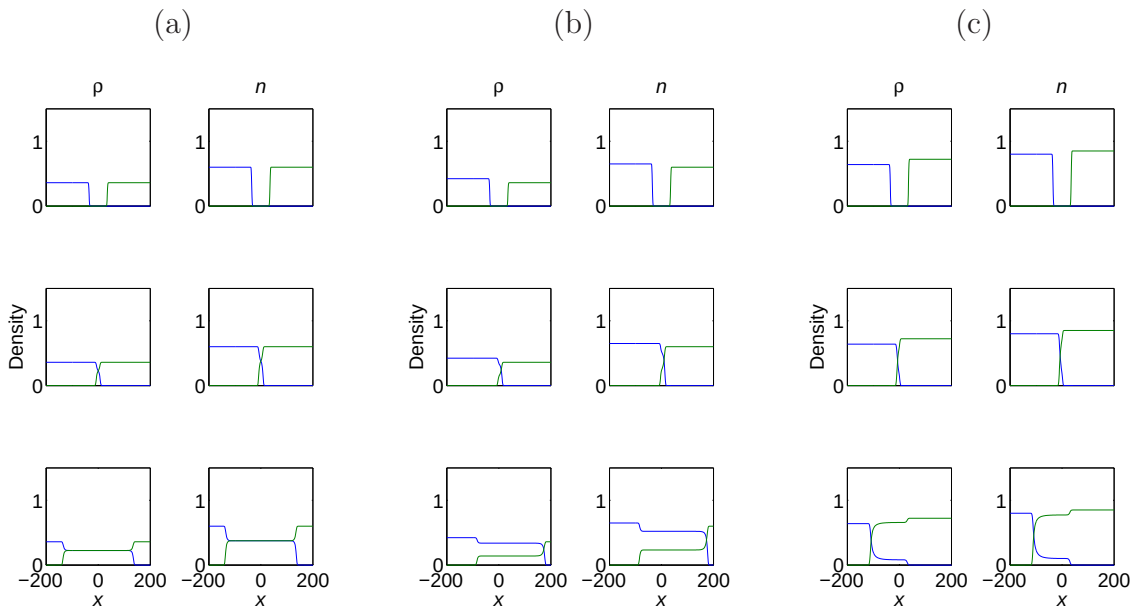

Figure 6: Numerical solutions of equations (3) with initial data (2),(4) over the interval $(-200, 200)$ with $\tilde{x} = 35$ and $A = B = 1$, $E = F = 0$ and $\psi = 10$. Distributions are shown at times $t = 0$, $t = 30$ and $t = 200$ for values of c_1 and c_2 in the region C of Fig. 1, ensuring coexistence (or intermingling) of biomasses. (a) $c_1 = 0.6$, $c_2 = 0.6$ (with travelling wave speeds of $s_1 = 2.07, s_2 = -2.07$ before collision, $s_1 = 0.77, s_2 = -0.77$ after collision). (b) $c_1 = 0.65$, $c_2 = 0.6$ (with travelling wave speeds of $s_1 = 2.27, s_2 = -2.07$ before collision, $s_1 = 0.98, s_2 = -0.49$ after collision). (c) $c_1 = 0.8$, $c_2 = 0.85$ (with travelling wave speeds of $s_1 = 2.92, s_2 = -3.07$ before collision, $s_1 = 0.18, s_2 = -0.61$ after collision).

$$\bar{\rho}_1 = \frac{Fc_1^3 - Ec_2^3 - 1 + \sqrt{\left(Fc_1^3 - Ec_2^3 - 1\right)^2 + 4Fc_1^3}}{2Fc_1}, \qquad \bar{n}_1 = c_1,$$

$$\bar{\rho}_2 = \frac{Ec_2^3 - Fc_1^3 - 1 + \sqrt{\left(Ec_2^3 - Fc_1^3 - 1\right)^2 + 4Ec_2^3}}{2Ec_2}, \qquad \bar{n}_2 = c_2,$$

and is asymptotically stable for all positive parameter values (see Appendix). Notice that $\bar{\rho}_1$ increases with c_1 but decreases with c_2 (and vice-versa for $\bar{\rho}_2$). Therefore the density of one model biomass increases with the availability of nutrients but is inhibited by the presence of a rival. Notice also that in this special case of $A = B = 0$, coexistence is always a stable stationary point and therefore the suppression of hyphal tips (which corresponds to $A, B > 0$) clearly occupies a central role in the diversity of outcomes of competition.

As in Section 3.1, and provided A and B are not both zero, the c_1-c_2 parameter space is divided by the curves $Bc_1^3(1 + Fc_1^3) = c_2^2$ and $Ac_2^3(1 + Ec_2^3) = c_1^2$ into the four regions found previously (Fig. 1). Hence if c_1 is significantly larger than c_2 the only stable equilibria corresponds to the presence of the model biomass ρ_1 and its model tips n_1, with the reverse case if c_2 is significantly larger than c_1. If c_1 and c_2 are both large then there are multiple

stable equilibria and provided c_1 and c_2 are sufficiently and similarly small then coexistence (i.e. intermingling) is observed.

As in the previous case, the existence of travelling wave solutions connecting the equilibria identified above can be determined by setting $z = x - st$ in equations (3) where A, B, E and F are non-zero:

$$\begin{aligned}
\rho_1' &= -\frac{1}{s}\left(c_1 n_1 - \rho_1 - E c_2 \rho_1 \rho_2\right), \\
n_1' &= -\frac{\psi}{s - c_1}\left(c_1 \rho_1 - \rho_1 n_1 - A c_2 n_1 \rho_2\right), \\
\rho_2' &= -\frac{1}{s}\left(c_2 n_2 - \rho_2 - F c_1 \rho_1 \rho_2\right), \\
n_2' &= -\frac{\psi}{s + c_2}\left(c_2 \rho_2 - \rho_2 n_2 - B c_1 n_2 \rho_1\right),
\end{aligned} \tag{8}$$

where prime denotes differentiation with respect to the wave variable z. Similar to the approach in Section 3.1 and for the same reasons, if ψ is large it is reasonable to make the approximations $n_1 = c_1\rho_1/(\rho_1 + Ac_2\rho_2)$, $n_2 = c_2\rho_2/(\rho_2 + Bc_1\rho_1)$ and hence the system of equations (8) reduce to

$$\begin{aligned}
\rho_1' &= -\frac{\rho_1}{s}\left(\frac{c_1^2}{\rho_1 + A c_2 \rho_2} - 1 - E c_2 \rho_2\right), \\
\rho_2' &= -\frac{\rho_2}{s}\left(\frac{c_2^2}{\rho_2 + B c_1 \rho_1} - 1 - F c_1 \rho_1\right),
\end{aligned} \tag{9}$$

and standard phase space analysis in the ρ_1-ρ_2 plane can be used to investigate this system. From equations (9), the ρ_2-nullclines are the line $\rho_2 = 0$ and the curve $\rho_2 = \dfrac{c_2^2}{1 + Fc_1\rho_1} - Bc_1\rho_1$, which is defined for all $\rho_1 \neq -1/(Fc_1)$. The second of these satisfies

$$\begin{aligned}
\frac{\mathrm{d}\rho_2}{\mathrm{d}\rho_1} &= -\frac{F c_1 c_2^2}{(1 + F c_1 \rho_1)^2} - B c_1, \\
\frac{\mathrm{d}^2\rho_2}{\mathrm{d}\rho_1^2} &= \frac{2F^2 c_1^2 c_2^2}{(1 + F c_1 \rho_1)^3}.
\end{aligned}$$

Notice that the first derivative of the non-zero nullcline is negative for all values of $\rho_1 \neq -1/(Fc_1)$ while the second derivative is positive provided $\rho_1 > -1/(Fc_1)$. In particular, this demonstrates that the non-zero ρ_2-nullcline decreases from the vertical asymptote $\rho_1 = -1/(Fc_1)$, crosses the ρ_2-axis at $(0, c_2^2)$ and tends to the oblique asymptote $\rho_2 = -Bc_1\rho_1$.

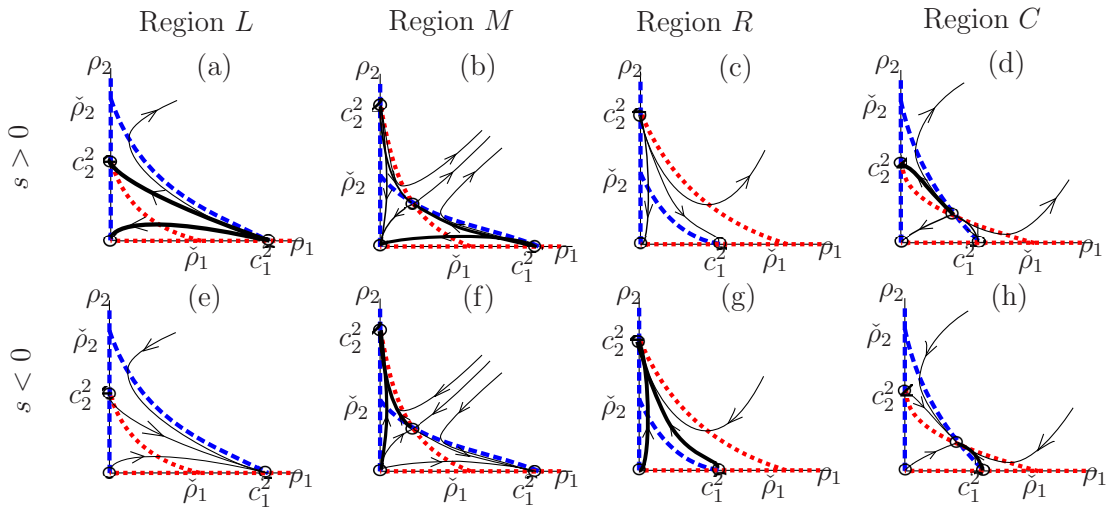

Figure 7: Phase portraits of equations (9) for the different regions of Fig. 1 where $s > 0$ and $s < 0$ as indicated. The ρ_1- and ρ_2-nullclines are represented by the dashed (blue) and dotted (red) lines respectively where $\check{\rho}_1 = (\sqrt{B^2 + 4BFc_2^2} - B)/(2BFc_1)$ and $\check{\rho}_2 = (\sqrt{A^2 + 4AEc_1^2} - A)/(2AEc_2)$. Sample trajectories are indicated along with specific trajectories (in bold) connecting equilibria illustrating biologically relevant travelling wave solutions of equations (3) for large ψ.

Through the symmetry in equations (9), the ρ_1-nullclines have equivalent properties where the model variables and parameters are suitably transposed; namely the non-zero ρ_1-nullcline has negative first derivative and positive second derivative provided $\rho_2 > -1/(Ec_2)$. In particular, in ρ_1-ρ_2 phase space, the non-zero ρ_1-nullcline declines from the oblique asymptote $\rho_2 = -\rho_1/(Ac_2)$, crosses the ρ_1-axis at $(c_1^2, 0)$ before tending to the horizontal asymptote $\rho_2 = -1/(Ec_2)$. Thus in the region $\rho_1 > -1/(Fc_1)$ and $\rho_2 > -1/(Ec_2)$ the non-zero ρ_1- and ρ_2-nullclines intersect precisely once. Depending on parameter values, this intersection may arise inside or outside the biologically relevant portion of the phase space (i.e. $\rho_1, \rho_2 \geq 0$). Consequently there are four ways the nullclines can intersect in the biologically-relevant portion of the phase space depending on parameter values but where the direction of flow depends on the sign of s generating a total of 8 distinct phase portraits (Fig. 7). This analysis demonstrates the existence of travelling wave solutions but, as in the case of the reduced system for large ψ in equations (7), no bounds on the wave speed can be obtained. Unfortunately, the case for small ψ does not yield any tractable analytical results.

The model equations (3) with initial data (2),(4) were solved numerically for a range of parameter values c_1 and c_2 (Fig. 8), with positive values used for all parameters and the speed of the travelling waves were calculated numerically before and after biomass collision. In all cases, the qualitative behaviour of the solutions were similar to that described in Section 3.1. In particular, for pairings of the parameters c_1 and c_2 in the region denoted by C in Fig. 1 where neither of the model biomasses in isolation were stable, the only observed outcome of competition was coexistence (or intermingling) of biomasses (Fig. 8(b)).

Furthermore, different pairings of the parameters c_1 and c_2 that lay within the multiple equilibria region M in Fig. 1 generated three distinct outcomes; the biomass initially starting on the right displaced that on the left (Fig. 8(d)), the biomasses reached a state of deadlock (Fig. 8(e)), and the biomass initially starting on the left displaced that on the right (Fig. 8(f)).

4. Discussion

In biotechnological applications that involve the introduction of a species of fungus to an environment, such as biological control and biological remediation, the interaction between it and other fungal species already present in the environment impacts on the success of the treatment. The current investigation has focused on how nutrient availability can influence the outcome of fungal interactions by altering the rate at which they degrade rival's hyphae and hyphal tips and the concomitant spatial reorganization. In particular, the mathematical model predicted the circumstances under which pairwise competition would result in the displacement of one species by another, the intermingling (or coexistence) of multiple species and the emergence of deadlock where a stalemate is reached.

In the instances of displacement or intermingling, the numerical solutions of the model equations suggested that the corresponding model biomasses advanced as a travelling wave. Indeed, through phase-space analysis, the existence of travelling wave solutions in the model equations were demonstrated for certain values of the parameter ψ, which essentially can be regarded as comparing the production of new biomass material through hyphal tip branching and extension to that lost through natural degradation. Furthermore, bounds on the travelling wave speed were also obtained in certain cases. Previous studies (Boswell et al., 2002; Boswell, 2012) have calibrated these parameter values for the fungus *Rhizoctonia solani* growing on a standard agar mixture from which ψ can be deduced to take values between 10^{12} and 10^{14}. Thus, since ψ is significantly larger than values taken by other parameters in the nondimensionalised model equations (3), there is strong experimental evidence to support the large ψ analysis used in the current investigation and the corresponding model equations essentially reduce to a pair of differential equations that exhibit Lotka-Volterra competition (e.g. Allen, 2007). However, the complete proof of the existence of travelling wave solutions for all values of ψ in equations (3), which involves proving the existence of heteroclinic trajectories in four-dimensional state space, remains an interesting open problem.

A key feature of the modelling was the distinction between the two major processes involved in fungal competition, namely the degradation of existing hyphae and the degradation of hyphal tips by rival fungi. The suppression of hyphal tips alone was shown to be a sufficient mechanism to generate the main observed behaviours in fungal interactions, i.e. displace-

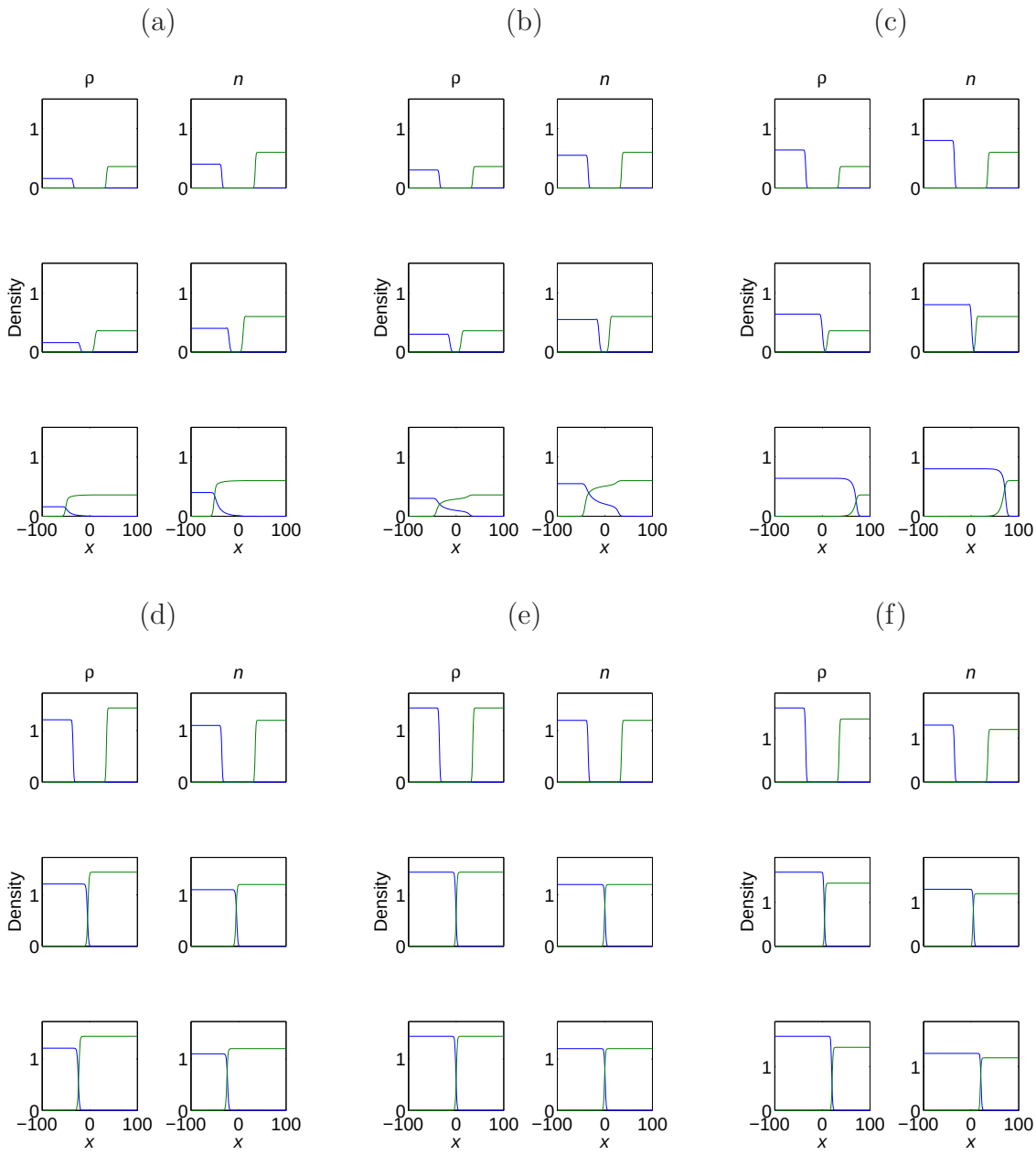

Figure 8: Numerical solutions of equations (3) with initial data (2),(4) over the interval $(-100, 100)$ with $\tilde{x} = 35$ and $\psi = A = B = E = F = 1$. Distributions are shown at times $t = 0$, $t = 30$ and $t = 100$ where c_1 and c_2 belong to regions (a) R, (b) C, (c) L, (d-f) M in Fig. 1. (a) $c_1 = 0.4$, $c_2 = 0.6$ (with travelling wave speeds of $s_1 = 0.54, s_2 = -0.86$ before collision, $s_1 = s_2 = -0.84$ after collision). (b) $c_1 = 0.55$, $c_2 = 0.6$ (with travelling wave speeds of $s_1 = 0.81, s_2 = -0.88$ before collision, $s_1 = 0.52, s_2 = -0.71$ after collision). (c) $c_1 = 0.8$, $c_2 = 0.6$ (with travelling wave speeds of $s_1 = 1.21, s_2 = -0.87$ before collision, $s_1 = s_2 = 1.03$ after collision). (d) $c_1 = 1.1$, $c_2 = 1.2$ (with travelling wave speeds of $s_1 = 1.75, s_2 = -1.94$ before collision, $s_1 = s_2 = -0.27$ after collision). (e) $c_1 = 1.2$, $c_2 = 1.2$ (with travelling wave speeds of $s_1 = 1.94, s_2 = -1.94$ before collision, $s_1 = s_2 = 0$ after collision). (f) $c_1 = 1.3$, $c_2 = 1.2$ (with travelling wave speeds of $s_1 = 2.24, s_2 = -1.94$ before collision, $s_1 = s_2 = 0.22$ after collision).

ment, intermingling and deadlock. Indeed, by not degrading hyphal tips, a mycelium was shown to be unable to completely displace its rival (Section 3.2 with $A = B = 0$) and therefore the only outcomes of competition with this singular regime are intermingling or its own displacement. Intuitively this is appealing: hyphal tip extension is the sole means by which mycelia expand and therefore the possibility of continued growth cannot be eliminated unless the hyphal tips are inhibited or degraded. However, the degradation of hyphal structures impacts on the ability of a mycelium to redistribute internally-held supplies, which is essential for continued growth, and therefore such degradation can reduce its ability to function effectively (e.g. Lee et al., 2017). This possibility cannot be captured in the current model because of its continuous nature, but hybrid approaches that explicitly simulate the discrete network of a mycelium have been used with some success (Boswell and Davidson, 2012). Nonetheless, our modelling has shown that hyphal degradation plays an important role in pairwise fungal competition; it significantly reduces the region of parameter space where intermingling (or coexistence) can arise and extends the regions corresponding to displacement (Fig. 1) and therefore provides a further competitive advantage to a fungus.
The modelling demonstrated that the availability of nutrients plays a central role on the outcomes of pairwise competition between fungal species. Coexistence, or intermingling, was shown to be possible only when the concentrations of nutrients provided to both model fungi were similarly small and deadlock was only possible when the nutrient concentrations were similarly large (Fig. 1). This result supports many of the findings in Boswell (2012) where numerical simulations showed that deadlock could arise when the suppression of hyphal tips and the degradation of biomass occurred at sufficiently large rates and coexistence arose when both rates were sufficiently small. However, in that study, the explicit dependence of nutrients on those two processes was neglected and instead the nutrients only influenced the branching and tip movement processes. Further, it was shown in Boswell (2012) that deadlock could be achieved when there was a significant disparity between nutrient availability in two fungal biomasses provided their tip suppression and hyphal degradation rates were also different. Our results in the current paper extend these findings; our modelling predicts that further increasing the nutrient disparity will change the outcome of competition resulting in the displacement of one biomass by another since it corresponds to the movement from region M in Fig. 1 to either region L or R, depending on the nutrient concentration changed. Indeed, additional numerical simulations using the model of Boswell (2012) have shown precisely this outcome (see Supplementary Material), thus demonstrating the additional insight gained from the current approach.
It has been shown in a number of experimental studies (e.g. Boddy, 1993, 2000) that under certain triggers, such as the presence of a rival biomass, fungi will construct structures, often termed barrages, to protect themselves. Such structures were not observed in our modelling and thus certain potential causes of these structures can be eliminated. In particular,

the degradation of hyphal tips (or biomass) by a rival fungus is not sufficient on its own to generate defensive structures; other mechanisms must be employed. These alternative mechanisms could potentially include a change in the redistribution of internally-located nutrients or a change in the movement habit of hyphal tips themselves in response to an anticipated attack. Such a change in the movement habit of tips may require additional spatial dimensions in the model, and consequently the basic structure of the model equations, especially tip flux and creation of biomass, would need careful revision, potentially by including their movement in response to different biomass distributions, see e.g. Boswell et al. (2003). Nonetheless, the modelling has demonstrated that fungi are better able to defend themselves when supplied with sufficient resources and hence the reallocation of internally-held resources to the colony periphery provides increased defensive capabilities for mycelia.

The distribution and concentration of nutrients has an essential role in the growth and function of fungi; in particular in their applications in bioremediation, pathogen neutralization and other biological control scenarios. In this study we have provided a simple yet powerful description of how nutrient concentrations can influence interactions between different fungi species. However, additional factors, including temperature (Hiscox et al., 2016) and water activity (Sempere and Santamarina, 2010) can influence the outcome of pairwise competition and so need to be incorporated into further models of fungal interactions.

Allen, L. J. S., 2007. An Introduction to Mathematical Biology. Pearson Education Ltd.

Balmant, W., Sugai-Guerios, M. H., Coradin, J. H., Krieger, N., Junior, A. F., Mitchell, D. A., 2015. A model for growth of a single fungal hypha based on well-mixed tanks: Simulation of nutrient and vesicle transport in aerial reproductive hyphae. PLoS One 10 (3), 1–22.

Boddy, L., 1993. Saprotrophic cord-forming fungi: warfare strategies and other ecological aspects. Mycological Research 97, 641–655.

Boddy, L., 1999. Saprotrophic cord-forming fungi: meeting the challenge of heterogeneous environments. Mycologia 91, 13–32.

Boddy, L., 2000. Interspecific combative interactions between wood-decaying basidiomycetes. FEMS Microbiology Ecology 31, 185–194.

Boswell, G., Davidson, F., 2012. Modelling hyphal networks. Fungal Biology Reviews 26, 30–38.

Boswell, G. P., 2012. Modelling combat strategies in fungal mycelia. Journal of Theoretical Biology 304, 226–234.

Boswell, G. P., Jacobs, H., Davidson, F. A., Gadd, G. M., Ritz, K., 2002. Functional consequences of nutrient translocation in mycelial fungi. Journal of Theoretical Biology 217 (4), 459–477.

Boswell, G. P., Jacobs, H., Davidson, F. A., Gadd, G. M., Ritz, K., 2003. Growth and function of fungal mycelia in heterogeneous environments. Bulletin of Mathematical Biology 65, 447–477.

Boswell, G. P., Jacobs, H., Ritz, K., Gadd, G., Davidson, F. A., 2007. The development of fungal networks in complex environments. Bulletin of Mathematical Biology 69, 605–634.

Bushley, K. E., Raja, R., Jaiswal, P., Cumbie, J. S., Nonogaki, M., Boyd, A. E., Owensby, C. A., Knaus, B. J., E., J., Miller, D., Di, Y., McPhail, K. L., Spatafora, J. W., 2013. The genome of *Tolypocladium inflatum*: Evolution, organization and expression of the cyclosporin biosynthetic gene cluster. PLOS Genetic DOI: 10.1371/journal.pgen.1003496, 1371.

Carlile, M. J., Watkinson, S. C., Gooday, G. W., 2001. The Fungi, 2$^{\text{nd}}$ Edition. Academic Press.

Cohen, D., 1967. Computer simulation of biological pattern generation processes. Nature 216, 246–248.

Cotty, P. J., Antilla, L., Wakelyn, P. J., 2007. Competitive exclusion of aflatoxin producers: farmer-driven research and development. In: Vincent, C., Goettel, M. S., Lazarovits, G. (Eds.), Biological control: a global perspective. CAB International, Oxfordshire, U.K., pp. 241–253.

Davidson, F. A., 1998. Modelling qualitative response of fungal mycelia to heterogeneous environments. Journal of Theoretical Biology 195, 281–292.

Davidson, F. A., 2007. Mathematical modelling of mycelia: a question of scale. Fungal Biology Reviews 21, 30–41.

Davidson, F. A., Boswell, G. P., Fischer, M. W. F., Heaton, L., Hofstadler, D., Roper, M., 2011. Mathematical modelling of fungal growth and function. IMA Fungus 2 (1), 33–37.

Davidson, F. A., Sleeman, B. D., Rayner, A. D. M., Crawford, J. W., Ritz, K., 1996. Context-dependent macroscopic patterns in growing and interacting mycelial networks. Proceedings of the Royal Society B: Biological Sciences 263, 873–880.

Dorner, J. W., Cole, R. J., Connick, W. J., Daigle, D. J., McGuire, M. R., Shasha, B. S., 2003. Evaluation of biological control formulations to reduce aflatoxin contamination in peanuts. Biological Control 26 (3), 318–324.

519 Edelstein, L., 1982. The propagation of fungal colonies: A model for tissue growth. Journal
520 of Theoretical Biology 98, 679–701.

521 Efiuvweuwere, B., Chynyere, M., 2001. The microbiology and deterioration of soft drinks
522 subjected to two different marketing. Global Journal of Pure and Applied Sciences 7(1),
523 43–48.

524 Evans, J. A., Eyre, C. A., Rogers, H. J., Boddy, L., Müller, C. T., 2008. Changes in volatile
525 production during interspecific interactions between four wood rotting fungi growing in
526 artificial media. Fungal Ecology 1, 57–68.

527 Falconer, R. E., Bown, J. L., White, N. A., Crawford, J. W., 2005. Biomass recycling and
528 the origin of phenotype in fungal mycelia. Proceedings. Biological sciences / The Royal
529 Society 272 (1573), 1727–1734.

530 Falconer, R. E., Bown, J. L., White, N. A., Crawford, J. W., 2008. Modelling interactions
531 in fungi. Journal of Royal Society Interface 5, 603–615.

532 Falconer, R. E., Bown, J. L., White, N. A., Crawford, J. W., 2011. Linking fungal individ-
533 uals to community scale patterns. Fungal Ecology 4, 76–82.

534 Ferguson, B. A., Dreisbach, T. A., Parks, C. G., Filip, G. M., Schmitt, C. L., 2003.
535 Coarsescale population structure of pathogenic *Armillaria* species in a mixed-conifer
536 forest in the Blue Mountains of Northeast Oregon. Canadian Journal of Forest Research
537 33, 612–623.

538 Flores-Maltos, A., Rodriguez-Duran, L. V., Renovato, J., Contreras, J. C., Rodriguez, R.,
539 Aguilar, C. N., 2011. Catalytical properties of free and immobilized *Aspergillus niger*
540 *Tannase*. Enzyme Research 2011, 768183.

541 Fuhr, M. J., Schubert, M., Schwarze, F., Herrmann, H. J., 2011. Modelling the hyphal
542 growth of the wood-decay fungus *Physisporinus vitreus*. Fungal Biology 115 (9), 919–
543 932.

544 Gooday, G., 1995. The dynamics of hyphal growth. Mycological Research 99, 385–394.

545 Gruhn, C. M., Gruhn, A. V., Miller, O. K., 1992. *Boletinellus merulioides* alters root
546 morphology of *Pinus densiflora* without mycorrhizal formation. Mycologia 84, 528–533.

547 Gupta, M., Shrivastava, S., 2014. Mycoremediation: A management tool for removal of
548 pollutants from environment. Indian Journal of Applied Research 4 (8), 289–291.

549 Halley, J. M., Comins, H. N., Lawton, J. H., Hassell, M. P., 1994. Competition, succession
550 and pattern in fungal communities: towards a cellular automata model. Oikos 70, 435–
551 442.

552 Hiscox, J., Clarkson, G., Savoury, M., Powell, G., Savva, I., Lloyd, M., Shipcott, J.,
553 Choimes, A., Cumbriu, X. A., Boddy, L., 2016. Effects of pre-colonisation and tem-
554 perature on interspecific fungal interactions in wood. Fungal Ecology 21, 32–42.

555 Hopkins, S., Boswell, G. P., 2012. Mycelial response to spatiotemporal nutrient heterogene-
556 ity: a velocity-jump mathematical model. Fungal Ecology 5, 124–136.

557 Horio, T., Oakley, B. R., 2005. The role of microtubules in rapid hyphal tip growth of
558 *Aspergillus nidulans*. Molecular Biology of the Cell 16(2), 918–926.

559 Hynes, J., Muller, C. T., Jones, T. H., Boddy, L., 2007. Changes in volatile production
560 during the course of fungal interactions between *hypholoma fasciculare* and *resinicium*
561 *bicolor*. Journal of Chemical Ecology 33, 43–57.

562 Jackson, S., Heath, I., 1993. Roles of calcium ions in hyphal tip growth. Microbiological
563 Reviews 57, 367–382.

564 Kennedy, P., 2010. Ectomycorrhizal fungi and interspecific competition: species interac-
565 tions, community structure, coexistence mechanism, and future research directions. New
566 Phytologist 187, 895–910.

567 Koutb, M., Ali, E. H., 2010. Potential of *Epicoccum purpurascens* strain 5615 AUMC as a
568 biocontrol agent of *Pythium irregulare* root rot in three leguminous plants. Mycobiology
569 38 (4), 286–294.

570 Lee, S. H., Fricker, M. D., Porter, M. A., 2017. Mesoscale analyses of fungal networks as an
571 approach for quantifying phenotypic traits. Journal of Complex Networks 5 (1), 145–159.

572 Luk, S., Lee, T., Liu, J., Lee, D. T., Chiu, Y. T., Ma, S., Ng, I., Wong, Y. C., Chan, F. L.,
573 Ling, M. T., 2011. Chemopreventive effect of psp through targeting of prostate cancer
574 stem cell-like population. PLos One 6 (5), 1–9.

575 Manjunathan, J., Subbulakshmi, N., Shanmugapriya, R., Kaviyarasan, V., 2011. Proximate
576 and mineral composition of four edible mushroom species from south india. International
577 Journal of Biodiversity and Conservation 3 (8), 386–388.

578 Mehl, H. L., Cotty, P. J., 2013. Nutrient environments influence competition among *As-*
579 *pergillus flavus* genotypes. Applied and Environmental Microbiology 79 (5), 1473–1480.

Meskauskas, A., Fricker, M., Moore, D., 2004a. Simulating colonial growth of fungi with the neighbour-sensing model of hyphal growth. Mycological Research 108 (11), 1241–1256.

Meskauskas, A., McNulty, L. J., Moore, D., 2004b. Concerted regulation of all hyphal tips generates fungal fruit body structures: experiments with computer visualizations produced by a new mathematical model of hyphal growth. Mycological Research 108 (4), 341–353.

Prosser, J. I., Trinci, A. P. J., 1979. A model for hyphal growth and branching. Journal of General Microbioloby 111, 153–164.

Ramachandran, R., Gnanados, J. J., 2013. Mycoremediation for the treatment of dye containing effluets. International Journal of Computing Algorithm 2, 286–293.

Sang, B.-I., Hori, K., Unno, H., 2004. A mathematical description for the fungal degradation process of biodegradable plastics. Mathematics and Computers in Simulation 65, 147–155.

Schmitz, H.-P., Kaufmann, A., Kohli, M., Laissue, P. P., Philippsen, P., 2006. From function to shape: a novel role of a formin in morphogenesis of the fungus *Ashbya gossypii*. Molecular Biology 17, 130–145.

Schnepf, A., Roose, T., Schweiger, P., 2008. Growth model for arbuscular mycorrhizal fungi. Journal of the Royal Society Interface 5(24), 773–784.

Selosse, M.-A., Richard, F., Xinhua, H., Simard, S. W., 2006. Mycorrhizal networks: des liaisons dangereuses? [mycorrhizal networks : the dangerous liaisons ?]. Trends in Ecology and Evolution 21(11), 621–628.

Sempere, F., Santamarina, M., 2010. Study of the interactions between *Penicillium oxalicum* Currie & Thom and *Alternaria alternata* (Fr.) Keissler. Brazilian Journal of Microbiology 41 (3), 700–706.

Smith, S. E., Read, D. J., 1997. Mycorrhizal Symbiosis, 2$^{\text{nd}}$ Edition. Academic Press.

Tlalka, M., Fricker, M., Watkinson, S., 2008. Imaging of long-distance α-aminoisobutyric acid translocation dynamics during resource capture by *Serpula lacrymans*. Applied and Environmental Microbiology 74, 2700–2708.

Torkelson, C. J., Sweet, E., Martzen, M. R., Sasagawa, M., Wenner, C. A., Gay, J., Putiri, A., Standish, L. J., 2012. Phase 1 clinical trial of *Trametes versicolor* in women with breast cancer. ISRN Oncology 2012, 251632.

Utermark, J., Karlovsky, P., 2007. Role of *Zearalenone lactonase* in protection of *Gliocladium roseum* from fungitoxic effects of the mycotoxin *Zearalenone*. Applied and Environmental Microbiology 73 (2), 637–642.

Vankudoth, K. R., Boda, A., Sivadevuni, G., Solipuram, M. R., 2016. Effect of indigenous fungi on ochratoxin A produced by two species of *Penicillium*. Animal Nutrition 2 (3), 225–228.

Yang, H., King, R., Reichu, U., Giles, E. D., 1992. Mathematical model for apical growth, septation, and branching of mycelial microorganisms. Biotechnology and Bioengineering 39(1), 49–58.

Appendix A

The spatially-uniform equilibria of the nondimensionalised equations (3) satisfy

$$\begin{aligned}
0 &= c_1 n_1 - \rho_1 - E c_2 \rho_1 \rho_2, \\
0 &= \psi(c_1 \rho_1 - \rho_1 n_1 - A c_2 n_1 \rho_2), \\
0 &= c_2 n_2 - \rho_2 - F c_1 \rho_1 \rho_2, \\
0 &= \psi(c_2 \rho_2 - \rho_2 n_2 - B c_1 \rho_1 n_2).
\end{aligned}$$

There are four equilibria, three of which can be easily determined after some trivial algebraic manipulation

$$\begin{aligned}
(\rho_1^*, n_1^*, \rho_2^*, n_2^*) = &(0,0,0,0), && \text{(SP0)} \\
&\left(c_1^2, c_1, 0, 0\right), && \text{(SP1)} \\
&\left(0, 0, c_2^2, c_2\right). && \text{(SP2)}
\end{aligned}$$

Clearly stationary points (SP0), (SP1) and (SP2) are biologically realistic (i.e. non-negative) for all non-negative parameter values. In general, the remaining stationary point, corresponding to coexistence, cannot be expressed in a convenient closed form. However, there are a number of exceptions and below we consider two important cases corresponding to the competition processes involved in the fungal interactions.

Under the special case $E = F = 0$, the coexistence stationary point can be explicitly determined:

$$(\rho_1^*, n_1^*, \rho_2^*, n_2^*) = \left(\frac{c_1^2(u-1)}{uw-1}, \frac{c_1(u-1)}{uw-1}, \frac{c_2^2(w-1)}{uw-1}, \frac{c_2(w-1)}{uw-1} \right), \qquad \text{(SP3a)}$$

where for convenience we have introduced $u = Ac_2^3/c_1^2$ and $w = Bc_1^3/c_2^2$. Further, it can be seen that the coexistence stationary point (SP3a) is biologically realistic when either $u, w > 1$ (corresponding to region M in Fig. 1) or $u, w < 1$ (corresponding to region C in Fig. 1).

In the second special case where $A = B = 0$, the coexistence stationary point is given by

$$(\rho_1^*, n_1^*, \rho_2^*, n_2^*) = \Bigg(\frac{Fc_1^3 - Ec_2^3 - 1 + \sqrt{\left(Fc_1^3 - Ec_2^3 - 1\right)^2 + 4Fc_1^3}}{2Fc_1}, c_1, \frac{Ec_2^3 - Fc_1^3 - 1 + \sqrt{\left(Ec_2^3 - Fc_1^3 - 1\right)^2 + 4Ec_2^3}}{2Ec_2}, c_2 \Bigg) \qquad \text{(SP3b)}$$

and is always biologically realistic for positive parameters.

The stability of the stationary points found above are determined from the Jacobian matrix

$$J(\rho_1, n_1, \rho_2, n_2) = \begin{bmatrix} -1 - Ec_2\rho_2 & c_1 & -Ec_2\rho_1 & 0 \\ \psi(c_1 - n_1) & -\psi\rho_1 - A\psi c_2\rho_2 & -A\psi c_2 n_1 & 0 \\ -Fc_1\rho_2 & 0 & -1 - Fc_1\rho_1 & c_2 \\ -B\psi c_1 n_2 & 0 & \psi(c_2 - n_2) & -\psi\rho_2 - B\psi c_1\rho_1 \end{bmatrix}$$

and the corresponding characteristic equations.

SP0

The characteristic equation obtained from the above Jacobian matrix evaluated at the stationary point $(0, 0, 0, 0)$ can be easily factorised into two quadratics

$$\left(\lambda^2 + \lambda - \psi c_2^2\right)\left(\lambda^2 + \lambda - \psi c_1^2\right) = 0.$$

Hence the stability of this stationary point is determined by the roots of two quadratic equations. Since the coefficient of the constant term is negative in at least one of the quadratics, the Routh-Hurwitz criteria for polynomials of degree 2 implies that there is an eigenvalue with a positive real part and hence the stationary point (SP0) is unstable. Furthermore, due to the structure of the quadratics, this stationary point is clearly a saddle point.

SP1

Substituting the equilibria $(c_1^2, c_1, 0, 0)$ into the above Jacobian matrix yields a characteristic equation that can be easily factorised:

$$(\lambda+1)(\lambda+\psi c_1^2)\left(\lambda^2+(1+Fc_1^3+\psi Bc_1^3)\lambda+\psi Bc_1^3(1+Fc_1^3)-\psi c_2^2\right)=0.$$

Since two of the eigenvalues are clearly negative, the roots of the quadratic determine the stability of stationary point (SP1). Again, using the Routh-Hurwitz criteria for polynomials of degree 2, the stationary point (SP1) is stable provided the constant term is positive, i.e. $Bc_1^3(1+Fc_1^3) > c_2^2$ and hence is otherwise a saddle point.

SP2

Similar to above, the characteristic equation evaluated at the stationary point (SP2) can be factorised:

$$(\lambda+1)(\lambda+\psi c_2^2)\left(\lambda^2+(1+Ec_2^3+\psi Ac_2^3)\lambda+\psi Ac_2^3(1+Ec_2^3)-\psi c_1^2\right)=0.$$

Hence an application of the Routh-Hurwitz criteria implies that stationary point (SP2) is stable provided $Ac_2^3(1+Ec_2^3) > c_1^2$ and is otherwise a saddle point.

SP3a

After significant algebraic manipulation, the characteristic equation of the above Jacobian matrix evaluated at the stationary point (SP3a) can be written as

$$\begin{aligned}(\lambda+1)\Bigg[\lambda^3+\left(1+\psi(c_1^2+c_2^2)\right)\lambda^2+\psi\left(\frac{c_1^2(u-1)+c_2^2(w-1)}{uw-1}+\psi c_1^2c_2^2\right)\lambda \\ -\psi^2c_1^2c_2^2\left(\frac{(u-1)(w-1)}{uw-1}\right)\Bigg]=0,\end{aligned} \tag{A.1}$$

where, as before, $u = Ac_2^3/c_1^2$ and $w = Bc_1^3/c_2^2$. Clearly $\lambda = -1$ is an eigenvalue and hence the roots of the remaining cubic determines the stability of the equilibria. Recall the stationary point (SP3a) is biologically realistic (i.e. the variables are non-negative) provided either $u, w > 1$ or $u, w < 1$. We investigate these two cases below but first recall from the Routh-Hurwitz criteria that the cubic equation $\lambda^3 + a\lambda^2 + b\lambda + c = 0$ has all roots with negative real parts if $a, b, c > 0$ and $ab - c > 0$.

With $u, w > 1$ the constant term in the cubic of equation (A.1) is negative and so the Routh-Hurwitz condition fails. Therefore the coexistence stationary point (SP3a) is unstable when $u, w > 1$.

Assuming $u, w < 1$ and then by examining the cubic in equation (A.1) it is easily seen that $a, b, c > 0$ is satisfied (i.e. the constant, linear and quadratic coefficients are all positive). The remaining condition for stability is investigated by examining the term $ab - c$ where a, b, c represent the quadratic, linear and constant coefficients respectively. After some lengthy algebra, the expression $ab - c$ can be written as

$$\left(\frac{c_1^2(u-1)+c_2^2(w-1)}{uw-1}\right)\psi+\left(\frac{c_1^4(u-1)+c_2^4(w-1)+2(uw-1)c_1^2c_2^2}{uw-1}\right)\psi^2+(c_1^4c_2^2+c_2^4c_1^2)\psi^3. \tag{A.2}$$

Since $u, w < 1$ and the remaining parameters are positive, it is clear that all three terms in (A.2) are positive. Therefore the Routh-Hurwitz criteria implies that the stationary point (SP3a) is stable provided $u, w < 1$, i.e. provided $Ac_2^3 < c_1^2$ and $Bc_1^3 < c_2^2$, and is otherwise a saddle point (or biologically unrealistic if it takes negative values).

SP3b

The characteristic equation of the above Jacobian matrix evaluated at the stationary point (SP3b) can be factorised to give

$$0 = (\lambda + \psi\rho_1^*)(\lambda + \psi\rho_2^*)(\lambda + 1)\,(\lambda + 1 + Ec_2\rho_2^* + Fc_1\rho_1^*)$$

where ρ_1^* and ρ_2^* are the values of ρ_1 and ρ_2 at the stationary point (SP3b) respectively. Clearly, since ρ_1^* and ρ_2^* are positive, the stationary point (SP3b) is asymptotically stable.